Casimir-Polder Interaction of an Atom with a Cavity Wall Made of Phase-Change Material out of Thermal Equilibrium

Galina L. Klimchitskaya [1,2] and Vladimir M. Mostepanenko [1,2,3,*]

1   Central Astronomical Observatory at Pulkovo of the Russian Academy of Sciences, 196140 Saint Petersburg, Russia; g.klimchitskaya@gmail.com
2   Institute of Physics, Nanotechnology and Telecommunications, Peter the Great Saint Petersburg Polytechnic University, 195251 Saint Petersburg, Russia
3   Kazan Federal University, 420008 Kazan, Russia
*   Correspondence: vmostepa@gmail.com

Abstract: We consider the out-of-thermal-equilibrium Casimir-Polder interaction between atoms of He*, Na, Cs, and Rb and a cavity wall made of sapphire coated with a vanadium dioxide film which undergoes the dielectric-to-metal phase transition with increasing wall temperature. Numerical computations of the Casimir-Polder force and its gradient as the functions of atom-wall separation and wall temperature are made when the latter exceeds the temperature of the environment. The obtained results are compared with those in experiment on measuring the gradient of the Casimir-Polder force between ^{87}Rb atoms and a silica glass wall out of thermal equilibrium. It is shown that the use of phase-change wall material significantly increases the force magnitude and especially the force gradient, as opposed to the case of a dielectric wall.

1. Introduction

The interaction of atoms with material surfaces is a long-explored area. At atom-surface separations exceeding one or two nanometers it is determined to a large extent by the zero-point and thermal fluctuations of the electromagnetic field. This is a particular case of the van der Waals forces which act between two atoms, an atom and a surface (or between two surfaces), and originate from fluctuating electric dipole moments [1]. The first theory of atom-surface interaction was created by London on the basis of nonrelativistic quantum mechanics [2]. It was generalized by taking into account an existence of the zero-point fluctuations and retardation of the electromagnetic interaction by Casimir and Polder, who studied a polarizable atom in the vicinity of an ideal metal wall [3]. Presently, the atom-wall force is often referred to by their names.

A more general theory taking into account the material properties of the wall at nonzero temperature in thermal equilibrium with the environment was developed in [4] on the basis of the Lifshitz theory [5,6]. In the framework of this theory, the free energy of the Casimir-Polder interaction and respective force were expressed via the frequency-dependent atomic polarizability and dielectric permittivity of the wall material. In succeeding years, the fluctuation-induced forces between atoms, molecules, and material surfaces found numerous applications in atomic physics, condensed matter physics, as well as in biology and chemistry [1,7]. The advent of magnetic traps and ultracold cooling has opened up new opportunities for detailed study of the Casimir-Polder force in high-precision experiments.

Thus, the phenomenon of quantum reflection, that is, a reflection of ultra-cold atoms under an action of the attractive atom-surface force was demonstrated for both liquid and solid surfaces [8–17]. Another phenomenon is the Bose-Einstein condensation in dilute

gases cooled to very low temperatures and confined in the magnetic trap near a material surface [18–22]. Although the Casimir-Polder force between a unit atom and a surface is extremely small and not directly measurable, it should be accounted for in precise experiments with atomic clouds involving an abundance of atoms. This stimulated applications of the Lifshitz theory to calculation of the Casimir-Polder force for different atoms and cavity walls, taking into account the atomic dynamic polarizabilities and dielectric properties of wall materials [23–45].

During the last few years, special attention was paid to the nonequilibrium Casimir-Polder forces which arise in situations when the surface (cavity wall) and the environment are kept at different temperatures. It is usually assumed that the temperature of the environment remains unchanged, whereas the cavity wall is heated to some higher temperature. The Casimir-Polder force under these conditions was discussed in [46], whereas the generalization of the Lifshitz theory to nonequilibrium situations, including the case of atom-wall interaction, was performed in [47,48]. This theory was used for interpretation of the measurement data of the experiment [49], where the thermal Casimir-Polder force between the ground state ^{87}Rb atoms, belonging to the Bose-Einstein condensate, and a silica glass wall heated up to 605 K was measured for the first time. The measure of agreement between the experimental data of [49] and theoretical predictions was used for constraining the Yukawa-type corrections to Newtonian gravity [50], and the coupling constants of axions to nucleons [51].

In this article, using the formalism of [47,48], we consider another physical situation where the nonequilibrium effects are gaining in importance, that is, the Casimir-Polder force between different atoms and subjected to a heating cavity wall which is made of the phase-change material. In fact, the equilibrium Casimir forces acting between a Au-coated sphere and either a VO$_2$ film deposited on a sapphire substrate [52] or a AgInSbTe film on a Si substrate [53] have already been considered in the literature. It has been known that VO$_2$ undergoes the phase transition from the dielectric to metallic phase with increasing temperature above $T_c = 341$ K. As to an amorphous AgInSbTe film, it undergoes the phase transition to the crystalline phase as a result of annealing. It was shown that the equilibrium Casimir force between a Au sphere and a VO$_2$ film experiences an abrupt jump resulting from the phase transition [52]. The same holds for the Casimir force between a sphere and an AgInSbTe film in different phase states [53]. Thus, it would be interesting to consider the combined effect of the nonequilibrium and phase-change conditions on the Casimir-Polder force for the wall material which undergoes phase transition with increasing temperature.

Here, we consider the atoms of metastable helium He*, Na, Rb, and Cs interacting with a VO$_2$ film deposited on a sapphire wall for the atom–film separations varying from 5 to 10 μm, as much as in the experiment [49] for ^{87}Rb atoms and a SiO$_2$ wall. We calculate the nonequilibrium Casimir-Polder forces for all these atoms at different wall temperatures, both below and above the critical temperature T_c at which the VO$_2$ film transforms from the dielectric to metallic phase, leaving the environmental temperature constant. It is shown that the magnitude of the Casimir-Polder force decreases monotonously with increasing atom-wall separation, but takes a much larger value at each separation if the wall temperature, although slightly, exceeds the critical temperature. When the atom-wall separation is fixed, the force magnitude increases monotonously with increasing wall temperature in the region $T < T_c$, experiences a jump at $T = T_c$, and increases further at $T > T_c$.

By way of example, for a Rb atom 5 μm apart from the wall made of the phase-change material, the magnitudes of equilibrium Casimir-Polder force at 300 K, 340 K (i.e., before the phase transition), and 342 K (i.e., after the phase transition) are equal to 1.92, 2.17, and 2.68 (10^{-13} fN), respectively. If, however, the environmental temperature remains equal to 300 K and only the wall is heated, one obtains the force magnitudes of 1.92, 5.05, and 8.29 (10^{-13} fN) at the same respective wall temperatures. We have also compared the nonequilibrium Casimir-Polder forces and their gradients between a Rb atom and either a VO$_2$ film on a sapphire wall, which undergoes the phase transition, or a dielectric SiO$_2$

wall employed in the experiment [49]. Using the experimental parameters, it is shown, for instance, that the nonequilibrium Casimir-Polder force between a Rb atom 7 μm apart from the wall made of the phase-change material reaches at $T = 415$ K wall temperature the same magnitude as is reached at $T = 605$ K in the case of a dielectric wall.

The structure of this article is the following. In Section 2, we briefly outline the used formalism. Section 3 contains the calculation results for the nonequilibrium Casimir-Polder force for different atoms and phase-change wall material as functions of atom-wall separation and wall temperature. In Section 4, the nonequilibrium Casimir-Polder force and its gradient for the phase-change wall material are compared with those for a dielectric wall used in the experimental configuration [49]. Section 5 contains a discussion of the obtained results. In Section 6, the reader will find our conclusions.

2. Nonequilibrium Casimir-Polder Force in the Micrometer Separation Range

Here, we summarize the main expressions, allowing calculation of the nonequilibrium force between a ground-state atom and a cavity wall spaced at separations of a few micrometers, obtained in [47,48]. In doing so, the atom is described by its static polarizability $\alpha(0)$, and the wall material by its dielectric properties at vanishing frequency. In the case of phase-change wall material, these properties are very specific and endow the nonequilibrium Casimir-Polder force with new and useful applications.

Let the temperature of the environment be $T_E = 300$ K, and the wall temperature be $T_W \geqslant T_E$. The atom-wall separation is denoted by a. Then the nonequilibrium Casimir-Polder force can be presented in the form [47,48]

$$F(a, T_W, T_E) = F_{\text{eq}}(a, T_E) + F_{\text{neq}}(a, T_W) - F_{\text{neq}}(a, T_E). \tag{1}$$

Here, F_{eq} is the well-known equilibrium Casimir-Polder force given by the Lifshitz formula, and F_{neq} is the proper nonequilibrium contribution. As is seen from (1), in the state of thermal equilibrium $T_W = T_E$, the nonequilibrium terms cancel each other out, and the Casimir-Polder force reduces to the equilibrium contribution alone.

The explicit expressions for both terms on the right-hand side of (1) at all separations can be found in [47,48] (see also the monograph [54]). Keeping in mind the values of the experimental parameters [49], here we deal with atom-wall separations in the region from 5 to 10 μm. In this region, one can obtain simple asymptotic expressions for both F_{eq} and F_{neq}. Thus, for an ideal dielectric wall possessing finite dielectric permittivity at zero frequency $\varepsilon(0) < \infty$, one has [54,55]

$$F_{\text{eq}}(a, T) = -\frac{3k_B T}{4a^4} \, \alpha(0) \, \frac{\varepsilon(0) - 1}{\varepsilon(0) + 1}, \tag{2}$$

where k_B is the Boltzmann constant.

It is common knowledge, however, that at any nonzero temperature, real dielectric materials possess some small conductivity (so-called dc conductivity) which vanishes with T exponentially fast [56,57]. As a result, for real dielectric materials, one obtains $\varepsilon(\omega) \to \infty$ when ω goes to zero, and instead of (2), one has

$$F_{\text{eq}}(a, T) = -\frac{3k_B T}{4a^4} \, \alpha(0). \tag{3}$$

The same result was derived for the equilibrium Casimir-Polder force between an atom and a metallic wall at separations exceeding a few micrometers. Note that (3) is given by the zero-frequency term of the Lifshitz formula. In so doing, the omitted sum over all nonzero Matsubara frequencies, which describes contribution of the zero-point oscillations to the force and some extra thermal contribution, is equal to 6.8% of (3) at $a = 5$ μm, $T = 300$ K, and quickly decreases with increasing separation and/or temperature.

Equations (2) and (3) invite some further information. The point is that measurements of the equilibrium Casimir force between a Au-coated sphere and a dielectric plate at

separations of a few hundred nanometers were found in disagreement with theoretical predictions of the Lifshitz theory if the dc conductivity of plate material is taken into account in computations [58–61]. An agreement between the theory and the measurement data is reached only if the dc conductivity is disregarded [58–61]. The measured equilibrium Casimir-Polder force is also in good agreement with theoretical predictions if the dc conductivity of the SiO₂ wall is omitted in computations [49], but excludes these predictions found with taken into account dc conductivity [62]. What is even more surprising is that the Casimir-Polder entropy corresponding to the equilibrium Casimir-Polder force found in the framework of the Lifshitz theory violates the Nernst heat theorem if the dc conductivity of the dielectric wall is included in calculation [63–67]. This conundrum is not yet resolved. Because of this, in the computations below, we consider both cases of taken into account and disregarded dc conductivity of the cavity wall at temperatures below T_c when VO₂ is in the dielectric phase.

A similar problem was revealed for the equilibrium Casimir force measured between the metallic sphere and metallic plate. It was found that theoretical predictions of the Lifshitz theory are excluded by the measurement data if the relaxation properties of conduction electrons are taken into account in calculations (see, e.g., [54,55,68,69] for a review and [70] for an attempts to solve this puzzle). For the interaction of nonmagnetic atoms with the metallic wall, however, the equilibrium Casimir-Polder force given by the Lifshitz formula does not depend on the relaxation properties of conduction electrons and, thus, the problem becomes immaterial.

Now, we consider the nonequilibrium contributions on the right-hand side of (1). At separations of a few micrometers between an atom and a dielectric wall, the asymptotic expression for F_{neq} was derived under a condition that the thermal frequency $\omega_T = k_B T / \hbar$ is much less than the characteristic frequency of the wall material [47,71] (see also review [72])

$$F_{\mathrm{neq}}(a, T) = -\frac{\pi \alpha(0)(k_B T)^2}{6c\hbar a^3} \frac{\varepsilon(0) + 1}{\sqrt{\varepsilon(0) - 1}}. \tag{4}$$

This result was obtained with disregarded dc conductivity of the dielectric wall $\sigma_0(T)$ connected with the dielectric permittivity according to

$$\varepsilon(\omega) = \varepsilon(0) + \frac{4\pi \mathrm{i} \sigma_0(T)}{\omega}. \tag{5}$$

We emphasize, however, that for the nonequilibrium contribution to the Casimir-Polder force, the inclusion in the calculation of the dc conductivity $\sigma_0(T) \ll \omega_T$ leads to practically the same values of F_{neq}, as are given in (4) [62]. This is distinct from the equilibrium contribution to the Casimir-Polder force between an atom and a dielectric wall.

For an atom interacting with a metallic wall possessing the conductivity $\sigma_m(T)$ under a condition $\omega_T \ll \sigma_0(T)$, it holds that [47]

$$F_{\mathrm{neq}}(a, T) = -\frac{\alpha(0)\zeta(3/2)\sqrt{\sigma_m(T)}\,(k_B T)^{3/2}}{c\sqrt{2\hbar}\,a^3}, \tag{6}$$

where $\zeta(z)$ is the Riemann zeta function. It should be stressed that this equation is derived by taking into account the relaxation properties of conduction electrons by means of the Drude model. If the relaxation properties of conduction electrons in metals are disregarded, the theoretically meaningless result for F_{neq} follows, which is also in contradiction with the measurement data. Because of this, one can conclude that the puzzling problems discussed above refer to only the Casimir and Casimir-Polder forces in a state of thermal equilibrium. Note also that following [47,71], we consider atoms in their ground states and assume that they cannot absorb the thermal radiation. Possible effects caused by the atomic absorption spectrum and radiation pressure are discussed in [72].

In the next sections, the above results are applied to different atoms interacting with a wall made of the phase-change material.

3. The Casimir-Polder Force between Different Atoms and VO$_2$ Film on a Sapphire Wall

Here, we consider the atoms of metastable He* and ground state Na, Rb, and Cs interacting with VO$_2$ film of thickness 100 nm deposited on a bulk sapphire wall. The atoms under consideration are characterized by their static atomic polarizabilities with the following values:

$$\alpha^{\text{He}^*}(0) = 4.678 \times 10^{-29} \text{ m}^3 \text{ [73,74]}, \quad \alpha^{\text{Na}}(0) = 2.411 \times 10^{-29} \text{ m}^3 \text{ [75]},$$
$$\alpha^{\text{Rb}}(0) = 4.73 \times 10^{-29} \text{ m}^3 \text{ [76]}, \quad \text{and} \quad \alpha^{\text{Cs}}(0) = 5.981 \times 10^{-29} \text{ m}^3 \text{ [75,77]}.$$

It is known that both vanadium dioxide (VO$_2$) crystals and thin films undergo the phase transition from dielectric, monoclinic, to a metallic tetragonal phase when the temperature increases up to $T_c = 341$ K [78]. The dielectric permittivity of VO$_2$ film that is 100 nm thick deposited on a sapphire wall was measured in the frequency region from 3.8×10^{14} to 7.6×10^{15} rad/s and fitted to the isotropic oscillator representation in [79,80] both before and after the phase transition.

According to the obtained results, the static dielectric permittivity of VO$_2$ film in the dielectric phase on a sapphire wall is equal to $\varepsilon(0) = 9.909$. The characteristic absorption frequency of a VO$_2$ film on a sapphire wall before the phase transition is of the order of 1.5×10^{15} rad/s—that is, it is much larger than the thermal frequency $\omega_T = 3.9 \times 10^{13}$ rad/s at room temperature $T = 300$ K and also at higher temperatures up to 600 K considered below. Because of this, Equation (4) is applicable in this case. The dc conductivity in the dielectric phase is of the order of $\sigma_0 \sim 10^{11}$ s^{-1}. In the region around room temperature, it is almost temperature-independent but goes to zero exponentially fast with vanishing T. As was noted in Section 2, an account of this conductivity does not make an impact on the result (4).

In the metallic phase at $T = 355$ K, the conductivity value of the film was measured to be $\sigma_m(T) = 2.03 \times 10^{15}$ s^{-1} [79], that is, by the four orders of magnitude higher than the dc conductivity in the dielectric phase. The conductivity $\sigma_m(T)$ is well-described in the framework of the Drude model as

$$\sigma_m(T) = \frac{\omega_p^2}{4\pi\gamma(T)}, \tag{7}$$

where $\omega_p = 5.06 \times 10^{15}$ rad/s is the plasma frequency and $\gamma(T = 355\,\text{K}) = 1.0 \times 10^{15}$ rad/s is the relaxation parameter. In the temperature region of our interest, the linear dependence of the relaxation parameter on T is determined by the electron-phonon interaction [81]

$$\gamma(T) = kT, \qquad k = \frac{1.0 \times 10^{15}}{355} \frac{\text{rad}}{\text{s K}}. \tag{8}$$

It is seen that for VO$_2$ film in a metallic phase, $\omega_T \ll \sigma_m(T)$ when T varies between 300 K and 600 K. Thus, the application condition of Equation (6) is satisfied.

Now, we compute the Casimir-Polder force between a Rb atom and a VO$_2$ film on a sapphire wall as a function of separation between them, assuming that the temperature of the environment is $T_E = 300$ K, whereas the wall temperature T_W is either equal to T_E (the situation of thermal equilibrium) or $T_W > T_E$ (the out-of-thermal-equilibrium situation)—specifically, $T_W = 340$ K, 345 K, and 385 K. In doing so, the first of these temperatures corresponds to a VO$_2$ film in the dielectric phase, whereas the next two, in the metallic phase.

The computational results for the force magnitude are shown in Figure 1 in the logarithmic scale as functions of separation by the lower and upper pairs of solid and dashed lines found at $T_W = T_E = 300$ K and $T_W = 340$ K, respectively, and by the two solid lines next to them computed at $T_W = 345$ K and 385 K. At thermal equilibrium (the lower pair of solid and dashed lines), the computations are made by Equations (2) and (3), respectively, with disregarded and taken into account dc conductivity. The upper pair of solid and dashed lines (out-of-thermal equilibrium situation, but VO$_2$ film is in the

dielectric phase) are computed by Equations (1), (2), (4), and (1), (3), (4), respectively, with disregarded and taken into account dc conductivity in the equilibrium contribution. The top two solid lines in Figure 1 (out-of-thermal-equilibrium situation, but VO$_2$ film is in the metallic phase) were computed by Equations (1), (3), and (6)–(8) at respective temperatures. Note that (6) and (8) take into account the dependence of the conductivity of metal on temperature as a parameter, as it should be done also for nonequilibrium Casimir force between two parallel plates [82].

As is seen in Figure 1, the magnitude of negative (attractive) Casimir-Polder force decreases with increasing atom-wall separation and increases with increasing temperature. If the dc conductivity is taken into account in computations (the dashed lines in the lower and upper pairs of lines related to a VO$_2$ film in the dielectric phase), the larger magnitudes of the Casimir-Polder force are obtained. There is a jump in the force magnitude in the temperature region from $T_W = 340$ K to 345 K, which includes the critical temperature $T_c = 341$ K of the phase transition.

To gain a better insight, in Figure 2 we present the same computational results for the magnitude of the Casimir-Polder force, as in Figure 1, times the factor $a^3/\alpha^{\text{Rb}}(0)$. This allows for plotting of the figure in a homogeneous scale, preserving the meaning and disposition of all lines. What is more, Figure 2 does not depend on the type of atom and gives the possibility to obtain the magnitudes of the nonequilibrium Casimir-Polder force for any atom interacting with a VO$_2$ film deposited on a sapphire wall, and specifically, for the atoms of He*, Na, and Cs. For this purpose, one should multiply the data of Figure 2 by the factor $\alpha(0)/a^3$ using the value of $\alpha(0)$ for the desirable atom.
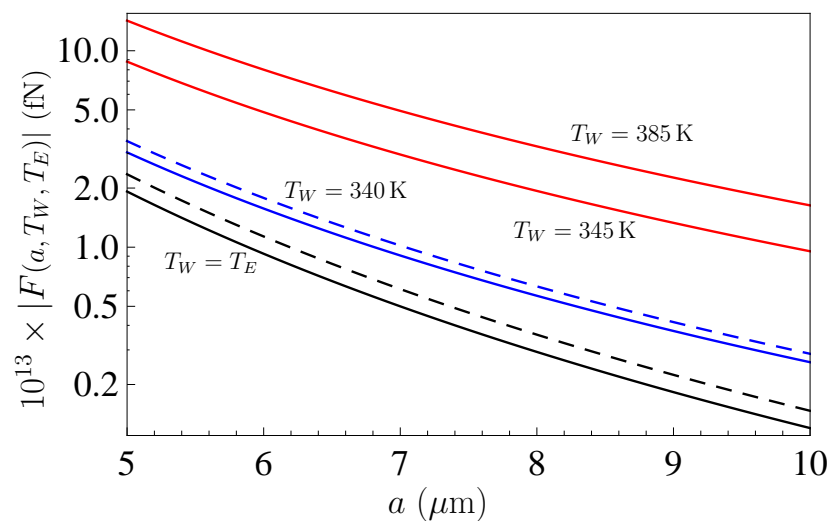

Figure 1. The magnitudes of the Casimir-Polder force between Rb atoms and VO$_2$ film on a sapphire wall are shown in the logarithmic scale by the solid and dashed lines as the functions of separation at the environmental temperature $T_E = 300$ K and the following wall temperatures T_W: $T_W = T_E$ (thermal equilibrium, the lower pair of solid and dashed lines computed with disregarded and taken into account dc conductivity, respectively), $T_W = 340$ K (out of thermal equilibrium, the upper pair of solid and dashed lines computed with disregarded and taken into account dc conductivity, respectively), $T_W = 345$ K (out of thermal equilibrium, metallic phase, the lower of two top solid lines), and $T_W = 385$ K (out of thermal equilibrium, metallic phase, the upper of two top solid lines).
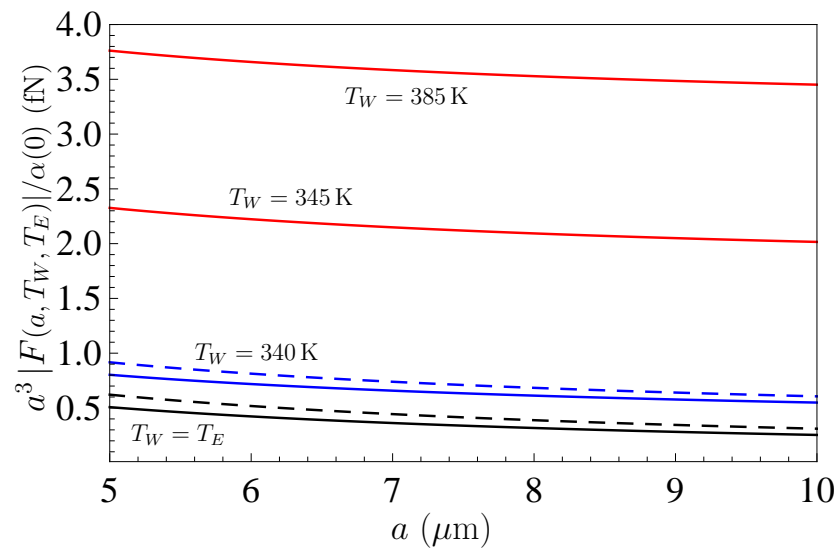
Figure 2. The magnitudes of the Casimir-Polder force between Rb atoms and VO$_2$ film on a sapphire wall times the factor $a^3/\alpha^{Rb}(0)$ are shown as the functions of separation at the environmental temperature $T_E = 300$ K and the following wall temperatures T_W: $T_W = T_E$ (thermal equilibrium, the lower pair of solid and dashed lines computed with disregarded and taken into account dc conductivity, respectively), $T_W = 340$ K (out of thermal equilibrium, the upper pair of solid and dashed lines computed with disregarded and taken into account dc conductivity, respectively), $T_W = 345$ K (out of thermal equilibrium, metallic phase, the lower of two top solid lines), and $T_W = 385$ K (out of thermal equilibrium, metallic phase, the upper of two top solid lines).

Now, using the same equations as explained above, we compute the nonequilibrium Casimir-Polder force between a Rb atom and a VO$_2$ film on a sapphire wall spaced at $a = 5$ μm separation as a function of wall temperature. The computational results are shown in Figure 3 by the lower pair of solid and dashed lines (wall temperature varies from 300 K to 340 K, VO$_2$ is in the dielectric phase, the dc conductivity is disregarded and taken into account, respectively) and by the bottom solid line (wall temperature varies from 342 K to 380 K, VO$_2$ is in the metallic phase). This computation is made at the environmental temperature $T_E = 300$ K. For comparison purposes, the upper pair of solid and dashed lines and the top solid line in the region of higher temperatures show similar equilibrium results computed under a condition $T_E = T_W$, that is, when the environment is heated up to the same temperature as the wall (measurement of the difference Casimir force in such a situation was proposed in [83]).

As is seen in Figure 3, the jump in the Casimir-Polder force due to the phase transition is much more pronounced in the nonequilibrium case than in the equilibrium one. Thus, the equilibrium Casimir-Polder force at room temperature ($T_E = T_W = 300$ K), just before the phase transition ($T_E = T_W = 340$ K) and just after the phase transition ($T_E = T_W = 342$ K) are equal to –1.92, –2.17, and –2.68 (10^{-13} fN), respectively (the dc conductivity in the dielectric phase is disregarded). If, however, the situation can be nonequilibrium, that is, $T_E = 300$ K, but $T_W = 300$ K, 340 K, and 342 K, one finds larger (in magnitude) values of the Casimir-Polder force –1.92, –5.05, and –8.29 (10^{-13} fN), respectively (the dc conductivity is again disregarded).

One more conclusion following from Figure 3 does not depend on whether the plate material undergoes the phase transition or is an ordinary dielectric or metal. In all these cases, the magnitude of the equilibrium Casimir-Polder force obtained when both the plate and the environment are heated up to some temperature $T > 300$ K is substantially smaller than the magnitude of the nonequilibrium force in the case when only the plate is heated up to the temperature T, whereas the environment preserves its temperature of 300 K.

The nonequilibrium Casimir-Polder force as a function of wall temperature was also computed for atoms of Na, He* and Cs spaced 5 μm apart of VO$_2$ film on a sapphire wall,

whereas the environment was kept at $T_E = 300$ K. The results are presented in Figure 4 in the same way as for Rb atoms in the nonequilibrium case in Figure 3. The three pairs of solid and dashed lines from top to bottom are for Na, He* and Cs atoms interacting with a VO_2 film in the dielectric phase (as above, the solid lines disregard dc conductivity and the dashed lines take it into account). The three solid lines from top to bottom are for the same respective atoms interacting with a VO_2 film in the metallic phase. In all these cases, the magnitude of the Casimir-Polder force increases significantly in out-of-thermal equilibrium conditions.
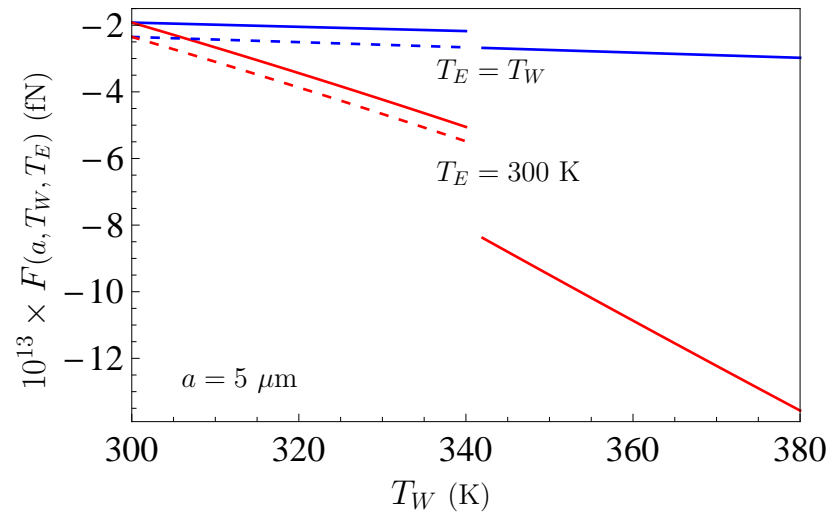

Figure 3. The Casimir-Polder forces between Rb atoms and VO_2 film on a sapphire wall at 5 μm separation are shown by the solid and dashed lines as the functions of wall temperature T_W in thermal equilibrium (the environmental temperature $T_E = T_W$, the upper pair of solid and dashed lines computed with disregarded and taken into account dc conductivity, respectively, and the top solid line for the metallic phase) and out of thermal equilibrium ($T_E = 300$ K, the lower pair of solid and dashed lines computed with disregarded and taken into account dc conductivity, respectively, and the bottom solid line for the metallic phase).
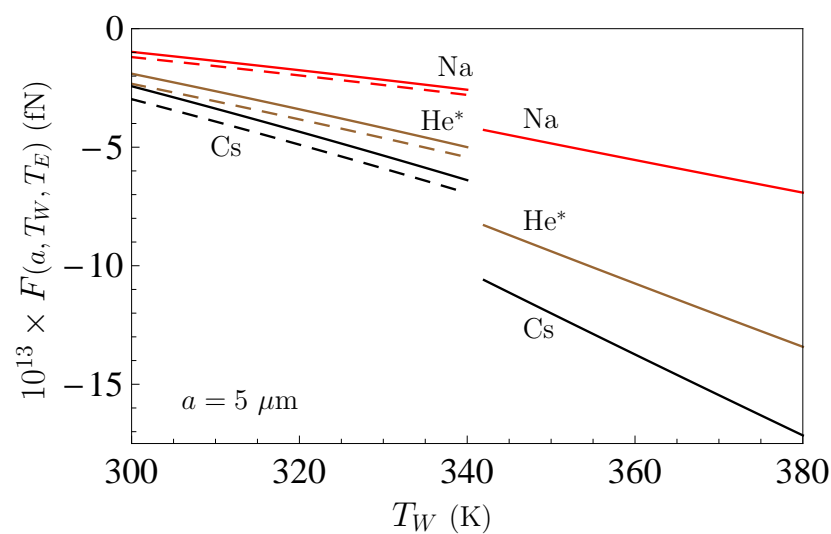

Figure 4. The nonequilibrium Casimir-Polder forces between Na, He*, and Cs atoms and VO_2 film on a sapphire wall at 5 μm separation are shown by the upper, middle, and lower pairs of solid and dashed lines, respectively, and respective solid lines as the functions of wall temperature at the environment temperature $T_E = 300$ K. The solid and dashed lines incorporated in pairs are computed with disregarded and taken into account dc conductivity, respectively.

4. Comparison between the Nonequilibrium Casimir-Polder Forces for the Phase-Change and Dielectric Materials

From Figures 1, 3, and 4, it is seen that both the equilibrium and nonequilibrium Casimir-Polder forces are extremely small. In fact, the forces below 1 fN are not accessible to a direct experimental observation. However, as noted in Section 1, the atom-wall forces lead to measurable effects in precise experiments, with atomic clouds incorporating a great number of atoms. Thus, the Bose–Einstein condensate of ^{87}Rb atoms was produced in a magnetic trap near a silica glass (SiO$_2$) surface and resonantly driven into a dipole oscillation [49]. It was shown [47,48] that both in the equilibrium ($T_W = T_E$) and nonequilibrium ($T_W > T_E$) situations, the Casimir-Polder forces lead to quite measurable shifts in the oscillation resonant frequency. These shifts were measured and recalculated into the gradients of the Casimir-Polder force [49].

Below, we compare the values of the nonequilibrium Casimir-Polder forces and their gradients, which were obtained in the experimental configuration [49] using the dielectric SiO$_2$ wall, with those found for the sapphire wall covered with a VO$_2$ film, which undergoes dielectric-to-metal phase transition with increasing temperature. The computations of the Casimir-Polder force in both cases were made using Equations (1)–(7), where the values of all necessary parameters are indicated above. For the static dielectric permittivity of SiO$_2$, one has $\varepsilon^{SiO_2}(0) = 3.8$ [84]. The temperature of the environment $T_E = 310$ K is used as in [49].

In Figure 5, the nonequilibrium Casimir-Polder forces between a Rb atom and a wall at 7 µm separation are shown as the functions of wall temperature by the upper pair of solid and dashed lines for a SiO$_2$ wall and by the lower pair of solid and dashed lines continued to higher temperatures by the bottom solid line for a VO$_2$ film deposited on a sapphire wall. In both cases, the solid and dashed lines incorporated in pairs are computed with disregarded and taken into account dc conductivity of a dielectric material, respectively. As is seen in Figure 5, in the case of phase-change wall material, the magnitudes of the Casimir-Polder force reach much larger values than for a dielectric SiO$_2$ wall. For example, at $T_W = 415$ K, the Casimir-Polder force between a Rb atom and a VO$_2$ film on a sapphire wall reaches the same magnitude as it reaches at $T_W = 605$ K in the case of a SiO$_2$ wall.
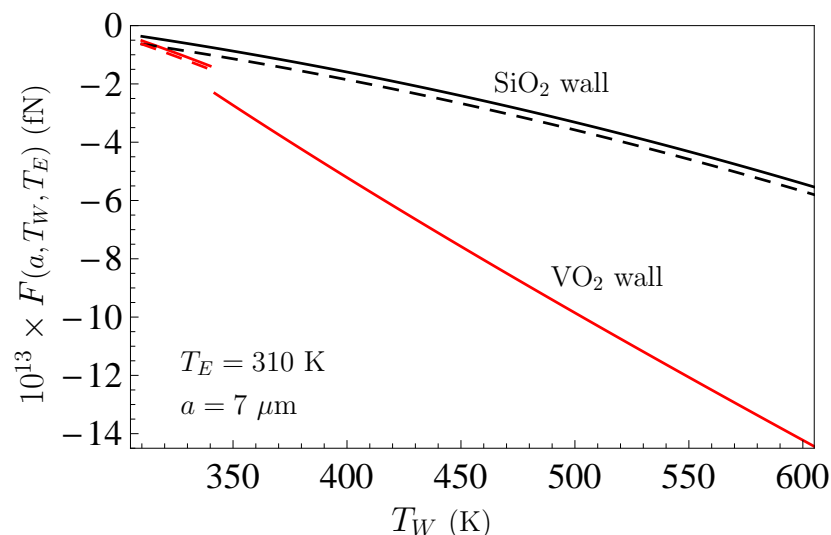

Figure 5. The nonequilibrium Casimir-Polder forces between Rb atoms and a wall at 7 µm separation are shown as the functions of wall temperature by the upper pair of solid and dashed lines for a SiO$_2$ wall and by the lower pair of solid and dashed lines continued to higher temperatures by the bottom solid line for a VO$_2$ film on a sapphire wall (the environmental temperature is $T_E = 310$ K). The solid and dashed lines incorporated in pairs are computed with disregarded and taken into account dc conductivity of dielectric materials.

In Figure 6, the comparison between the Casimir-Polder forces in the cases of phase-change and dielectric walls is made on an enlarged scale in the vicinity of the transition temperature $T_c = 341$ K. It is seen that although the phase transition contributes essentially to the magnitude of the Casimir-Polder force at $T > T_c$, the slope of the force lines for a phase-change wall is, in any case, larger than for a dielectric wall. This makes the phase-change wall material preferable for measurements of the nonequilibrium Casimir-Polder force in precise experiments.
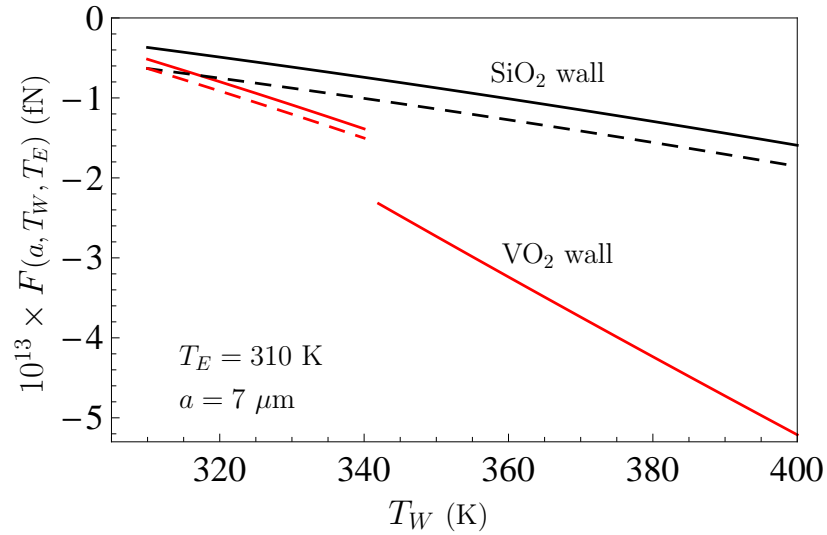

Figure 6. The nonequilibrium Casimir-Polder forces between Rb atoms at 7 μm separation from the wall, made either of SiO_2 or sapphire coated with VO_2 film are shown as the functions of wall temperature in the vicinity of the critical temperature. All notations are the same as in the caption of Figure 5.

To confirm this conclusion, we also compare the gradients of the Casimir-Polder forces between Rb atoms and either the VO_2 on sapphire or SiO_2 walls, taking into account that the force gradients are directly connected with the measured frequency shift [49]. The gradient of the nonequilibrium Casimir-Polder force is obtained by differentiating (1) with respect to separation

$$F'(a, T_W, T_E) = F'_{eq}(a, T_E) + F'_{neq}(a, T_W) - F'_{neq}(a, T_E). \tag{9}$$

Here, the equilibrium contribution to the force gradient for a dielectric wall with disregarded dc conductivity is obtained from (2)

$$F'_{eq}(a, T) = \frac{3k_B T}{a^5} \alpha(0) \frac{\varepsilon(0) - 1}{\varepsilon(0) + 1} \tag{10}$$

and with taken into account dc conductivity from (3)

$$F'_{eq}(a, T) = \frac{3k_B T}{a^5} \alpha(0). \tag{11}$$

The last result is also valid for a wall material in the metallic phase.

The nonequilibrium contribution to (9) is obtained from (4) for a dielectric wall

$$F'_{neq}(a, T) = \frac{\pi \alpha(0)(k_B T)^2}{2c\hbar a^4} \frac{\varepsilon(0) + 1}{\sqrt{\varepsilon(0) - 1}}, \tag{12}$$

and from (6) for a metallic wall

$$F'_{\text{neq}}(a, T) = \frac{3\alpha(0)\zeta(3/2)\sqrt{\sigma_m(T)}\,(k_B T)^{3/2}}{c\sqrt{2\hbar}\,a^4}. \tag{13}$$

Computations of the gradient of the nonequilibrium Casimir-Polder force between a Rb atom and either a SiO_2 wall or a VO_2 film on a sapphire wall at 7 µm separation were made by Equations (9)–(13). The computational results are shown in Figure 7 as the functions of wall temperature by the lower pair of solid and dashed lines for a SiO_2 wall and by the upper pair of solid and dashed lines continued to higher temperatures by the top solid line for a VO_2 film deposited on a sapphire wall. In both cases, the solid and dashed lines incorporated in pairs are computed with disregarded and taken into account dc conductivity of the dielectric material, respectively. The environmental temperature $T_E = 310$ K is used in computations. In the inset, the range of temperatures in the vicinity of the critical temperature $T_c = 341$ K, at which the phase transition occurs, is shown on an enlarged scale.
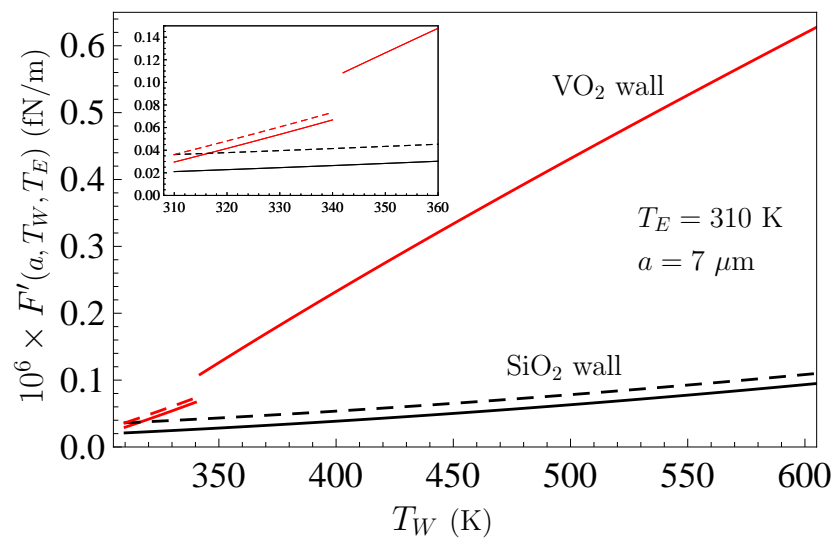

Figure 7. The gradients of nonequilibrium Casimir-Polder forces between Rb atoms and a wall at 7 µm separation are shown as the functions of wall temperature by the lower pair of solid and dashed lines for a SiO_2 wall and by the upper pair of solid and dashed lines continued to higher temperatures by the top solid line for a VO_2 film on a sapphire wall (the environmental temperature is $T_E = 310$ K). The solid and dashed lines incorporated in pairs are computed with disregarded and taken into account dc conductivity of dielectric materials. The temperature region in the vicinity of the critical temperature is shown in the inset on an enlarged scale.

As is seen in Figure 7, in the case of a VO_2 film on a sapphire wall, one obtains much larger gradients of the nonequilibrium Casimir-Polder force than for a SiO_2 wall under the same conditions. Thus, at $T_W = 350$ K and 400 K, the gradients of the Casimir-Polder force for a VO_2 film on a sapphire wall exceed those for a SiO_2 wall by factors of 4.46 and 6.02, respectively. The value of the force gradient reached in the experiment [49] at $T_W = 605$ K would be reached for a VO_2 film on a sapphire wall at a much lower temperature, $T_W = 342$ K, just after the phase transition (compared with 415 K found for the respective values of the magnitude of the Casimir-Polder force in Figure 5). This confirms that the use of phase-change wall materials is advantageous in experiments involving measuring the nonequilibrium Casimir-Polder forces.

5. Discussion

In the foregoing, we have considered the Casimir-Polder interaction between different atoms and a wall in an out-of-thermal-equilibrium situation when the wall temperature differs from the temperature of the environment. The Lifshitz theory of the fluctuation-induced forces has already been generalized for this case [47,48], and the nonequilibrium Casimir-Polder force was measured in the pioneer experiment [49]. The main novel feature of our study is a suggestion to use the material of the wall which undergoes the dielectric-to-metal phase transition with increasing wall temperature.

We have considered He*, Na, Rb, and Cs atoms interacting with a VO_2 film deposited on a sapphire wall. The question arises on what is an advantage of vanadium dioxide as compared with silica glass (SiO_2) used in the already performed measurements of the nonequilibrium Casimir-Polder force. The point is that at relatively low temperatures $T = 341$ K, vanadium dioxide undergoes a transition from the dielectric to metallic phase, accompanied by a jump in its conductivity by the four orders of magnitude. As a result, the Casimir-Polder force is subjected to a combined action of the nonequilibrium conditions and the phase transformation. Our calculations of the nonequilibrium Casimir-Polder force as a function of atom-wall separation and wall temperature show that in the case of phase change wall material, the force magnitude reaches much larger values at the same separation and temperature than in the case of a dielectric wall.

A comparison of this kind was made not only for the Casimir-Polder force, but for its gradient as well, taking into account that just the gradient is connected with the immediately measured shift in the oscillation resonant frequency of the condensate atomic cloud in [49]. It is shown that the combined action of the thermal nonequilibrium and phase transition on the force gradient is even more pronounced than on the Casimir-Polder force. As an example, at 7 μm atom-wall separation and 400 K wall temperature, the force gradient for the phase change wall material is by a factor of 6 greater than for a dielectric wall (whereas the force magnitude in the same case is greater only by a factor of 3). This opens up new opportunities for experimental investigation of atom-wall interaction in out-of-thermal-equilibrium conditions.

6. Conclusions

To conclude, in spite of extremely small magnitudes of the Casimir-Polder forces acting between separate atoms and cavity walls, they lead to important effects which are observable in such physical phenomena as quantum reflection and Bose–Einstein condensation dealing with clouds embodying the great number of cold atoms. The use of out-of-thermal-equilibrium conditions enhances the capabilities for investigation of atom-wall interaction. We have shown that heating of the wall alone by keeping the environmental temperature constant leads to larger magnitudes of the nonequilibrium Casimir-Polder force, as compared to the equilibtium ones obtained when both the wall and the environment are heated up to the same temperature. According to our results, even more prospective possibilities for research in the area of Casimir-Polder forces are presented by the combined use of nonequilibrium conditions and phase-change wall materials.

Author Contributions: Investigation, both authors; writing, both authors. All authors have read and agreed to the published version of the manuscript.

Institutional Review Board Statement: Not applicable.

Informed Consent Statement: Not applicable.

Data Availability Statement: In this theoretical work all the necessary data are provided in the text.

Conflicts of Interest: The authors declare no conflict of interest.

References

1. Parsegian, V.A. *Van der Waals Forces: A Handbook for Biologists, Chemists, Engineers, and Physicists*; Cambridge University Press: Cambridge, UK, 2005.
2. London, F. Zur Theorie und Systematik der Molecularkräfte. *Z. Phys.* **1930**, *63*, 245–279. [CrossRef]
3. Casimir, H.B.G.; Polder, D. The influence of retardation on the London-van der Waals forces. *Phys. Rev.* **1948**, *73*, 360–372. [CrossRef]
4. Dzyaloshinskii, I.E.; Lifshitz, E.M.; Pitaevskii, L.P. The general theory of van der Waals forces. *Usp. Fiz. Nauk* **1961**, *73*, 381–422 (*Adv. Phys.* **1961**, *10*, 165–209). [CrossRef]
5. Lifshitz, E.M. The theory of molecular attractive forces between solids. *Zh. Eksp. Teor. Fiz.* **1955**, *29*, 94–110; Reprint in *Sov. Phys. JETP* **1956**, *2*, 73–83.
6. Lifshitz, E.M.; Pitaevskii, L.P. *Statistical Physics, Part II*; Pergamon: Oxford, UK, 1980.
7. Mahanty, J.; Ninham, B.W. *Dispersion Forces*; Academic: London, UK, 1976.
8. Nayak, V.U.; Edwards, D.O.; Masuhara, N. Scattering of ^{4}He Atoms Grazing the Liquid- ^{4}He Surface. *Phys. Rev. Lett.* **1983**, *50*, 990–993. [CrossRef]
9. Berkhout, J.J.; Luiten, O.J.; Setija, I.D.; Hijmans, T.W.; Mizusaki, T.; Walraven, J.T.M. Quantum reflection: Focusing of hydrogen atoms with a concave mirror. *Phys. Rev. Lett.* **1989**, *63*, 1689–1693. [CrossRef]
10. Doyle, J.M.; Sandberg, J.C.; Yu, I.A.; Cesar, C.L.; Kleppner, D.; Greytak, T.J. Hydrogen in the submillikelvin regime: Sticking probability on superfluid ^{4}He. *Phys. Rev. Lett.* **1991**, *67*, 603–607. [CrossRef]
11. Yu, I.A.; Doyle, M.J.; Sandberg, J.C.; Cesar, C.L.; Kleppner, D.; Greytak, T.J. Evidence for universal quantum reflection of hydrogen from liquid ^{4}He. *Phys. Rev. Lett.* **1993**, *71*, 1589–1593. [CrossRef]
12. Shimizu, F. Specular Reflection of Very Slow Metastable Neon Atoms from a Solid Surface. *Phys. Rev. Lett.* **2001**, *86*, 987–991. [CrossRef]
13. Friedrich, H.; Jacoby, G.; Meister, C.J. Quantum reflection by Casimir-van der Waals potential tails. *Phys. Rev. A* **2002**, *65*, 032902. [CrossRef]
14. Druzhinina, V.; DeKieviet, M. Experimental Observation of Quantum Reflection far from Threshold. *Phys. Rev. Lett.* **2003**, *91*, 193202. [CrossRef] [PubMed]
15. Oberst, H.; Tashiro, Y.; Shimizu, K.; Shimizu, F. Quantum reflection of He* on silicon. *Phys. Rev. A* **2005**, *71*, 052901. [CrossRef]
16. Judd, T.E.; Scott, R.G.; Martin, A.M.; Kaczmarek, B.; Fromhold, T.M. Quantum reflection of ultracold atoms from thin films, graphene and semiconductor heterostructures. *New J. Phys.* **1983**, *13*, 083020. [CrossRef]
17. Rojas-Lorenzo, G.; Rubayo-Soneira, J.; Miret-Artés, S.; Pollak, E. Influence of realistic atom wall potentials in quantum reflection traps. *Phys. Rev. A* **2007**, *75*, 022902.
18. Harber, D.M.; McGuirk, J.M.; Obrecht, J.M.; Cornell, E.A. Thermally Induced Losses in Ultra-Cold Atoms Magnetically Trapped Near Room-Temperature Surfaces. *J. Low Temp. Phys.* **2003**, *133*, 229–238. [CrossRef]
19. Leanhardt, A.E.; Shin, Y.; Chikkatur, A.P.; Kielpinski, D.; Ketterle, W.; Pritchard, D.E. Bose-Einstein Condensates Near a Microfabricated Surface. *Phys. Rev. Lett.* **2003**, *90*, 100404. [CrossRef] [PubMed]
20. Harber, D.M.; Obrecht, J.M.; McGuirk, J.M.; Cornell, E.A. Measurement of the Casimir-Polder force through center-of-mass oscillations of a Bose-Einstein condensate. *Phys. Rev. A* **2005**, *72*, 033610. [CrossRef]
21. Lin, Y.-j.; Teper, I. Chin, C.; Vuletić, V. Impact of the Casimir-Polder Potential and Johnson Noise on Bose-Einstein Condensate Stability Near Surfaces. *Phys. Rev. Lett.* **2004**, *92*, 050404. [CrossRef]
22. Pethick, C.; Smith, H. *Bose-Einstein Condensation in Dilute Gases*; Cambridge University Press: Cambridge, UK, 2014.
23. Babb, J.F.; Klimchitskaya, G.L.; Mostepanenko, V.M. Casimir-Polder interaction between an atom and a cavity wall under the influence of real conditions. *Phys. Rev. A* **2004**, *70*, 042901. [CrossRef]
24. Antezza, M.; Pitaevskii, L.P.; Stringari, S. Effect of the Casimir-Polder force on the collective oscillations of a trapped Bose-Einstein condensate. *Phys. Rev. A* **2004**, *70*, 053619. [CrossRef]
25. Caride, A.O.; Klimchitskaya, G.L.; Mostepanenko, V.M.; Zanette, S.I. Dependences of the van der Waals atom-wall interaction on atomic and material properties. *Phys. Rev. A* **2005**, *71*, 042901. [CrossRef]
26. Babb, J.F. Long-range atom-surface interactions for cold atoms. *J. Phys. Conf. Ser.* **2005**, *19*, 001. [CrossRef]
27. Mostepanenko, V.M.; Babb, J.F.; Caride, A.O.; Klimchitskaya, G.L.; Janette, S.I. Dependence of the Casimir-Polder interaction between atom and a cavity wall on atomic and material properties. *J. Phys. A Math. Gen.* **2006**, *39*, 6583–6588. [CrossRef]
28. Blagov, E.V.; Klimchitskaya, G.L.; Mostepanenko, V.M. van der Waals interaction between a microparticle and a single-walled carbon nanotube. *Phys. Rev. B* **2007**, *75*, 235413. [CrossRef]
29. Bezerra, V.B.; Klimchitskaya, G.L.; Mostepanenko, V.M.; Romero, C. Lifshitz theory of atom-wall interaction with applications to quantum reflection. *Phys. Rev. A* **2008**, *78*, 042901. [CrossRef]
30. Safari, H.; Welsch, D.-G.; Buhmann, S.Y.; Scheel, S. van der Waals potentials of paramagnetic atoms. *Phys. Rev. A* **2008**, *78*, 062901. [CrossRef]

31. Bimonte, G.; Klimchitskaya, G.L.; Mostepanenko, V.M. Impact of magnetic properties on atom-wall interactions. *Phys. Rev. A* **2009**, *79*, 042906. [CrossRef]

32. Haakh, H.; Intravaia, F.; Henkel, C.; Spagnolo, S.; Passante, R.; Power, B.; Sols, F. Temperature dependence of the magnetic Casimir-Polder interaction. *Phys. Rev. A* **2009**, *80*, 062905. [CrossRef]

33. Ellingsen, S.Å.; Buhmann, S.Y.; Scheel, S. Temperature-Independent Casimir-Polder Forces Despite Large Thermal Photon Numbers. *Phys. Rev. Lett.* **2010**, *104*, 223003. [CrossRef]

34. Chaichian, M.; Klimchitskaya, G.L.; Mostepanenko, V.M.; Tureanu, A. Thermal Casimir-Polder interaction of different atoms with graphene. *Phys. Rev. A* **2012**, *86*, 012515. [CrossRef]

35. Passante, R.; Rizzuto, L.; Spagnolo, S.; Tanaka, S.; Petrosky, T.Y. Harmonic oscillator model for the atom-surface Casimir-Polder interaction energy. *Phys. Rev. A* **2012**, *85*, 062109. [CrossRef]

36. Ribeiro, S.; Scheel, S. Shielding vacuum fluctuations with graphene. *Phys. Rev. A* **2013**, *88*, 042519; Erratum in **2014**, *89*, 039904(E). [CrossRef]

37. Arora, B.; Kaur, H.; Sahoo, B.K. C_3 coefficients for the alkali atoms interacting with a graphene and carbon nanotube. *J. Phys. B* **2014**, *47*, 155002. [CrossRef]

38. Kaur, K.; Kaur, J.; Arora, B.; Sahoo, B.K. Emending thermal dispersion interaction of Li, Na, K and Rb alkali-metal atoms with graphene in the Dirac model. *Phys. Rev. B* **2014**, *90*, 245405. [CrossRef]

39. Klimchitskaya, G.L.; Mostepanenko, V.M. Classical Casimir-Polder force between polarizable microparticles and thin films including graphene. *Phys. Rev. A* **2014**, *89*, 012516. [CrossRef]

40. Klimchitskaya, G.L.; Mostepanenko, V.M. Impact of graphene coating on the atom-plate interaction. *Phys. Rev. A* **2014**, *89*, 062508. [CrossRef]

41. Knusnutdinov, N.; Kashapov, R.; Woods, L.M. Casimir-Polder effect for a stack of conductive planes. *Phys. Rev. A* **2016**, *94*, 012513. [CrossRef]

42. Fuchs, S.; Crosse, J.A.; Buhmann, S.Y. Casimir-Polder shift and decay rate in the presence of nonreciprocal media. *Phys. Rev. A* **2017**, *95*, 023805. [CrossRef]

43. Fuchs, S.; Bennett, R.; Krems, R.V.; Buhmann, S.Y. Nonadditivity of Optical and Casimir-Polder Potentials. *Phys. Rev. Lett.* **2018**, *121*, 083603. [CrossRef]

44. Bordag, M.; Klimchitskaya, G.L.; Mostepanenko, V.M. Nonperturbative theory of atom-surface interaction: Corrections at short separations. *J. Phys. Condens. Matter* **2018**, *30*, 055003. [CrossRef]

45. Henkel, C.; Klimchitskaya, G.L.; Mostepanenko, V.M. Influence of the chemical potential on the Casimir-Polder interaction between an atom and gapped graphene or a graphene-coated substrate. *Phys. Rev. A* **2018**, *97*, 032504. [CrossRef]

46. Henkel, C.; Joulain, K.; Mulet, J.P.; Greffet, J.J. Radiation forces on small particles in thermal near fields. *J. Opt. A Pure Appl. Opt.* **2002**, *4*, S109–114. [CrossRef]

47. Antezza, M.; Pitaevskii, L.P.; Stringari, S. New Asymptotic Behavior of the Surface-Atom Force out of Thermal Equilibrium. *Phys. Rev. Lett.* **2005**, *95*, 113202. [CrossRef]

48. Antezza, M.; Pitaevskii, L.P.; Stringari, S.; Svetovoy, V.B. Casimir-Lifshitz force out of thermal equilibrium. *Phys. Rev. A* **2008**, *77*, 022901. [CrossRef]

49. Obrecht, J.M.; Wild, R.J.; Antezza, M.; Pitaevskii, L.P.; Stringari, S.; Cornell, E.A. Measurement of the temperature dependence of the Casimir-Polder force. *Phys. Rev. Lett.* **2007**, *98*, 063201. [CrossRef] [PubMed]

50. Bezerra, V.B.; Klimchitskaya, G.L.; Mostepanenko, V.M.; Romero, C. Advance and prospects in constraining the Yukawa-type corrections to Newtonian gravity from the Casimir effect. *Phys. Rev. D* **2010**, *81*, 055003. [CrossRef]

51. Bezerra, V.B.; Klimchitskaya, G.L.; Mostepanenko, V.M.; Romero, C. Constraints on the parameters of an axion from measurements of the thermal Casimir-Polder force. *Phys. Rev. D* **2014**, *89*, 035010. [CrossRef]

52. Castillo-Garza, R.; Chang, C.-C.; Jimenez, D.; Klimchitskaya, G.L.; Mostepanenko, V.M.; Mohideen, U. Experimental approaches to the difference in the Casimir force due to modifications in the optical properties of the boundary surface. *Phys. Rev. A* **2007**, *75*, 062114. [CrossRef]

53. Torricelli, G.; van Zwol, P.J.; Shpak, O.; Binns, C.; Palasantzas, G.; Kooi, B.J.; Svetovoy, V.B.; Wuttig, M. Switching Casimir forces with phase-change materials. *Phys. Rev. A* **2010**, *82*, 010101(R). [CrossRef]

54. Bordag, M.; Klimchitskaya, G.L.; Mohideen, U.; Mostepanenko, V.M. *Advances in the Casimir Effect*; Oxford University Press: Oxford, UK, 2015.

55. Klimchitskaya, G.L.; Mohideen, U.; Mostepanenko, V.M. The Casimir force between real materials: Experiment and theory. *Rev. Mod. Phys.* **2009**, *81*, 1827–1885. [CrossRef]

56. Shklovskii, B.I.; Efros, A.L. *Electronic Properties of Doped Semiconductors*; Springer: Berlin, Germany, 1984.

57. Mott, N.F. *Metal–Insulator Transitions*; Taylor and Francis: London, UK, 1990.

58. Chen, F.; Klimchitskaya, G.L.; Mostepanenko, V.M.; Mohideen, U. Demonstration of optically modulated dispersion forces. *Opt. Express* **2007**, *15*, 4823–4829. [CrossRef] [PubMed]

59. Chen, F.; Klimchitskaya, G.L.; Mostepanenko, V.M.; Mohideen, U. Control of the Casimir force by the modification of dielectric properties with light. *Phys. Rev. B* **2007**, *76*, 035338. [CrossRef]

60. Chang, C.C.; Banishev, A.A.; Klimchitskaya, G.L.; Mostepanenko, V.M.; Mohideen, U. Reduction of the Casimir Force from Indium Tin Oxide Film by UV Treatment. *Phys. Rev. Lett.* **2011**, *107*, 090403. [CrossRef]

61. Banishev, A.A.; Chang, C.C.; Castillo-Garza, R.; Klimchitskaya, G.L.; Mostepanenko, V.M.; Mohideen, U. Modifying the Casimir force between indium tin oxide film and Au sphere. *Phys. Rev. B* **2012**, *85*, 045436. [CrossRef]

62. Klimchitskaya, G.L.; Mostepanenko, V.M. Conductivity of dielectric and thermal atom-wall interaction. *J. Phys. A Math. Theor.* **2008**, *41*, 312002. [CrossRef]

63. Geyer, B.; Klimchitskaya, G.L.; Mostepanenko, V.M. Thermal quantum field theory and the Casimir interaction between dielectrics. *Phys. Rev. D* **2005**, *72*, 085009. [CrossRef]

64. Klimchitskaya, G.L.; Mohideen, U.; Mostepanenko, V.M. Casimir-Polder interaction between an atom and a dielectric plate: Thermodynamics and experiment. *J. Phys. A Math. Theor.* **2008**, *41*, 432001. [CrossRef]

65. Klimchitskaya, G.L.; Korikov, C.C. Casimir entropy for magnetodielectrics. *J. Phys. Condens. Matter* **2015**, *27*, 214007. [CrossRef]

66. Klimchitskaya, G.L.; Mostepanenko, V.M. Casimir free energy of dielectric films: Classical limit, low-temperature behavior and control. *J. Phys. Condens. Matter* **2017**, *29*, 275701. [CrossRef]

67. Korikov, C.C.; Mostepanenko, V.M. Nernst heat theorem for the Casimir-Polder interaction between a magnetizable atom and ferromagnetic dielectric plate. *Mod. Phys. Lett. A* **2020**, *35*, 2040010. [CrossRef]

68. Bimonte, G.; López, D.; Decca, R.S. Isoelectronic determination of the thermal Casimir force. *Phys. Rev. B* **2016**, *93*, 184434. [CrossRef]

69. Woods, L.M.; Dalvit, D.A.R.; Tkatchenko, A.; Rodriguez-Lopez, P.; Rodriguez, A.W.; Podgornik, R. Materials perspective on Casimir and van der Waals interactions. *Rev. Mod. Phys.* **2016**, *88*, 045003. [CrossRef]

70. Klimchitskaya, G.L.; Mostepanenko, V.M. An alternative response to the off-shell quantum fluctuations: A step forward in resolution of the Casimir puzzle. *Eur. Phys. J. C* **2020**, *80*, 900. [CrossRef]

71. Antezza, M. Surface-atom force out of thermal equilibrium and its effect on ultra-cold atoms. *J. Phys. A Math. Gen.* **2006**, *39*, 6117–6126. [CrossRef]

72. Intravaia, F.; Henkel, C.; Antezza, M. Fluctuation-Induced Forces Between Atoms and Surfaces: The Casimir-Polder Interaction. In *Casimir Physics*; Dalvit, D., Milonni, P., Roberts, D., da Rosa, F., Eds.; Springer: Heidelberg, Germany, 2011; pp. 345–391.

73. Yan, Z.-C.; Babb, J.F. Long-range interactions of metastable helium atoms. *Phys. Rev. A* **1998**, *58*, 1247–1252. [CrossRef]

74. Brühl, R.; Fouquet, P.; Grisenti, R.E.; Toennies, J.P.; Hegerfeldt, G.C.; Köhler, T.; Stoll, M.; Walter C. The van der Waals potential between metastable atoms and solid surfaces: Novel diffraction experiments vs. theory. *Europhys. Lett.* **2002**, *59*, 357–363. [CrossRef]

75. Derevianko, A.; Johnson, W.R.; Safronova, M.S.; Babb, J.F. High-Precision Calculations of Dispersion Coefficients, Static Dipole Polarizabilities, and atom-wall interaction Constants for Alkali-Metal Atoms. *Phys. Rev. Lett.* **1999**, *82*, 3589–3593. [CrossRef]

76. Safronova, M.S.; Williams, C.J.; Clark, C.W. Relativistic many-body calculations of electric-dipole matrix elements, lifetimes, and polarizabilities in rubidium. *Phys. Rev. A* **2004**, *69*, 022509. [CrossRef]

77. Derevianko, A.; Porsev, S.G. Determination of lifetimes of $6P_J$ levels and ground-state polarizability of Cs from the van der Waals coefficient C_6. *Phys. Rev. A* **2002**, *65*, 053403. [CrossRef]

78. Zylbersztejn, A.; Mott, N.F. Metal-insulator transition in vanadium dioxide. *Phys. Rev. B* **1975**, *11*, 4383–4395. [CrossRef]

79. Verleur, H.W.; Barker, A.S., Jr.; Berglund, C.N. Optical Properties of VO_2 between 0.25 and 5 eV. *Phys. Rev.* **1968**, *172*, 788–798. [CrossRef]

80. Verleur, H.W. Determination of optical constants from reflectance or transmission measurements of bulk crystals or thin films. *J. Opt. Soc. Am.* **1968**, *58*, 1356–1364. [CrossRef]

81. Ashcroft, N.W.; Mermin, N.D. *Solid State Physics*; Saunders Colledge: Philadelphia, PA, USA, 1976.

82. Ingold, G.-L.; Klimchitskaya, G.L.; Mostepanenko, V.M. Nonequilibrium effects in the Casimir force between two similar metallic plates kept at different temperatures. *Phys. Rev. A* **2020**, *101*, 032506. [CrossRef]

83. Chen, F.; Klimchitskaya, G.L.; Mohideen, U.; Mostepanenko, V.M. New Features of the Thermal Casimir Force at Small Separations. *Phys. Rev. Lett.* **2003**, *90*, 160404. [CrossRef]

84. Hough, D.B.; White, L.H. The calculation of Hamaker constant from Lifshitz theory with application to wetting phenomena. *Adv. Colloid Interface Sci.* **1980**, *14*, 3–41. [CrossRef]